A Combined Local and Nonlocal Closure Model for the Atmospheric Boundary Layer. Part I: Model Description and Testing

JONATHAN E. PLEIM

Atmospheric Sciences Modeling Division, Air Resources Laboratory, National Oceanic and Atmospheric Administration, Research Triangle Park, North Carolina*

(Manuscript received 21 February 2006, in final form 11 September 2006)

ABSTRACT

The modeling of the atmospheric boundary layer during convective conditions has long been a major source of uncertainty in the numerical modeling of meteorological conditions and air quality. Much of the difficulty stems from the large range of turbulent scales that are effective in the convective boundary layer (CBL). Both small-scale turbulence that is subgrid in most mesoscale grid models and large-scale turbulence extending to the depth of the CBL are important for the vertical transport of atmospheric properties and chemical species. Eddy diffusion schemes assume that all of the turbulence is subgrid and therefore cannot realistically simulate convective conditions. Simple nonlocal closure PBL models, such as the Blackadar convective model that has been a mainstay PBL option in the fifth-generation Pennsylvania State University–National Center for Atmospheric Research Mesoscale Model (MM5) for many years and the original asymmetric convective model (ACM), also an option in MM5, represent large-scale transport driven by convective plumes but neglect small-scale, subgrid turbulent mixing. A new version of the ACM (ACM2) has been developed that includes the nonlocal scheme of the original ACM combined with an eddy diffusion scheme. Thus, the ACM2 is able to represent both the supergrid- and subgrid-scale components of turbulent transport in the convective boundary layer. Testing the ACM2 in one-dimensional form and comparing it with large-eddy simulations and field data from the 1999 Cooperative Atmosphere–Surface Exchange Study demonstrates that the new scheme accurately simulates PBL heights, profiles of fluxes and mean quantities, and surface-level values. The ACM2 performs equally well for both meteorological parameters (e.g., potential temperature, moisture variables, and winds) and trace chemical concentrations, which is an advantage over eddy diffusion models that include a nonlocal term in the form of a gradient adjustment.

1. Introduction

The limitations of local eddy diffusion models for representing convective conditions in the planetary boundary layer (PBL) are well known. The basic problem is that eddy diffusion assumes that the turbulent eddies are of a smaller scale than the vertical grid spacing of the model. Thus, modeled fluxes are proportional to local gradients. The convective boundary layer (CBL), however, is characterized by buoyant plumes originating in the surface layer and rising up into the capping inversion. Thus, the subgrid assumption of eddy diffusion is not valid and fluxes are often counter to the local gradients. For example, upward heat flux typically penetrates to ~80% of the PBL height (h), while potential temperature gradients are very small through most of the PBL and are often counter to the flux in the upper half of the PBL.

Nonlocal closure schemes have been successful at simulating convective boundary layer fluxes and profiles. Many PBL schemes simply add a gradient adjustment term (γ_h) to the eddy diffusion equation (Deardorff 1966; Troen and Mahrt 1986; Holtslag and Boville 1993; Noh et al. 2003),

$$\frac{\partial \theta}{\partial t} = \frac{\partial}{\partial z}\left(\overline{w'\theta'}\right) = \frac{\partial}{\partial z}\left[-K_h\left(\frac{\partial \theta}{\partial z} - \gamma_h\right)\right], \qquad (1)$$

where K_h is the vertical eddy diffusivity for heat, θ is the potential temperature, and $\overline{w'\theta'}$ represents the kinematic heat flux. Note that these schemes were originally

* In partnership with the U.S. Environmental Protection Agency.

Corresponding author address: Jonathan Pleim, Atmospheric Sciences Modeling Division, Air Resources Laboratory, NOAA, Research Triangle Park, NC 27711.
E-mail: pleim.jon@epa.gov

DOI: 10.1175/JAM2539.1

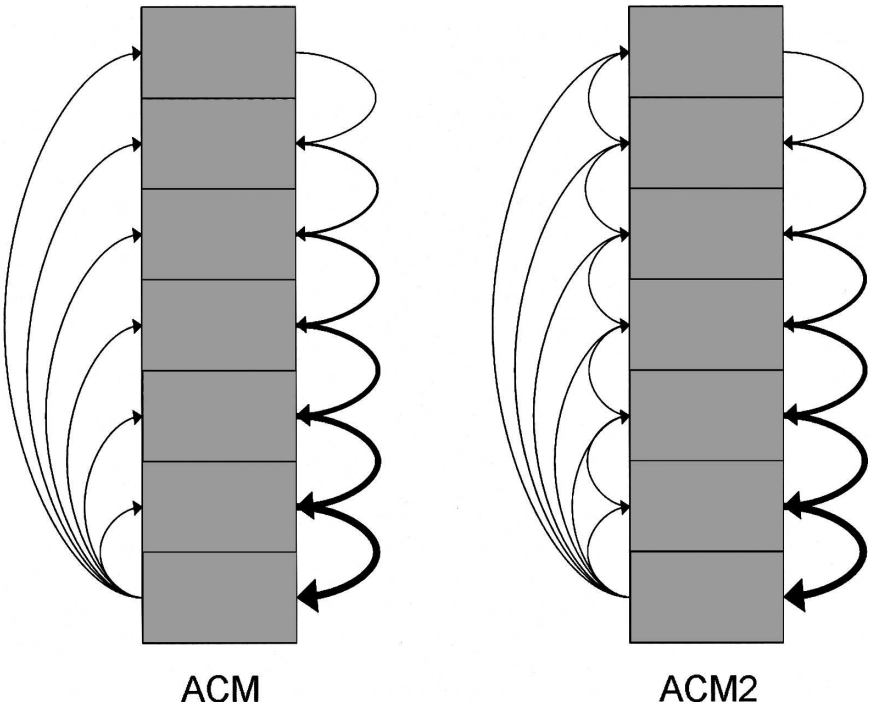

FIG. 1. Schematic representations of the exchange among model layers in the original ACM1 and the ACM2.

developed for heat flux, and application of the countergradient term to other quantities has been problematic. Other PBL schemes represent nonlocal fluxes explicitly using a transilient matrix that defines the mass flux between any pair of model layers even if they are not adjacent (e.g., Stull 1984; Blackadar 1978; Pleim and Chang 1992):

$$\frac{\partial \theta_i}{\partial t} = \sum_j M_{ij}\theta_j\,, \tag{2}$$

where M_{ij} is the transilient matrix containing the mixing coefficients between layers i and j.

The original asymmetrical convective model (ACM1; Pleim and Chang 1992) is a simple transilient model with a very sparse, efficient semi-implicit matrix solver. The ACM1 is a modification of the Blackadar convective model (Blackadar 1978), which prescribes convective transport as originating in the lowest model layer, representing the surface layer, and rising directly to all other layers within the CBL with symmetrical return flow from each layer back to the lowest layer. The principal modification for the ACM1 was to replace the symmetrical downward transport with an asymmetrical layer-by-layer downward transport. Thus, mass fluxes are represented in the ACM1 by rapid upward transport in convectively buoyant plumes and gradual downward transport due to compensatory subsidence (Fig. 1a). The ACM1 has been used in the fifth-generation Pennsylvania State University–National Center for Atmospheric Research Mesoscale Model (MM5; Grell et al. 1994) as part of the Pleim–Xiu land surface model (PX-LSM), and is an option for PBL treatment in the Community Multiscale Air Quality (CMAQ) model (Byun and Schere 2006).

A drawback of the original ACM1 is that it has no facility for local upward diffusion, resulting in an unrealistic step function from the first to the second model layers. This approach seemed reasonable for mesoscale meteorological and air-quality modeling when the ACM1 was first developed in the late 1980s, but as vertical resolution increases with faster computers there seems to be a need for more sophisticated models that produce more realistic vertical profiles.

The new ACM, version 2, (ACM2) adds an eddy diffusion component to the nonlocal transport. With the addition of the eddy diffusion component, the ACM2 can better represent the shape of the vertical profiles, especially the gradually decreasing gradient near the surface. Thus, the ACM2 can represent potential temperature profiles similarly to eddy diffusion schemes with the gradient adjustment term, but because local and nonlocal mass fluxes are explicitly defined, the ACM2 is more applicable to other quantities

(e.g., humidity, winds, or trace chemical mixing ratios). Thus, the purpose of the ACM2 is to provide a realistic and computationally efficient PBL model for use in both meteorological and atmospheric-chemistry models. Note that consistent treatment of meteorological and chemical species is becoming increasingly important as more applications involve online coupling of meteorological and chemical components.

The development, testing, and evaluation of the ACM2 are presented in a series of articles. This work presents the development, mathematical description, and 1D offline testing of the model. Pleim (2007, hereinafter Part II) describes MM5 simulations using the ACM2 and evaluation of results for a 1-month period in the summer of 2004. A third and forthcoming article will present the application and evaluation of CMAQ simulations using ACM2 for the same period and evaluation of chemical concentration profiles in comparison with aircraft measurements from the International Consortium for Atmospheric Research on Transport and Transformation (ICARTT) study. The ACM2 is also being included into the Weather Research and Forecast (WRF) model.

2. Model formulation

The new model is a combination of local and nonlocal closure. In specific terms, the ACM2 is a combination of the original ACM1 (Pleim and Chang 1992) and eddy diffusion. The key technique is to match the two schemes at a certain height, in this case the top of the lowest model layer, and apportion the mixing rate between the two schemes so that the resultant flux at that height is identical to that produced by either scheme running alone. Note that a reasonably high vertical grid resolution is required, such that the top of the lowest layer can be considered to be within the surface layer. While sensitivity tests have show some dependence on resolution, particularly in the shape of the lowest part of the profile, the scheme has proven to be robust using the lowest layer thicknesses, ranging from 50 m for the large-eddy simulation (LES) tests shown in section 3a, down to 4 m for the Global Energy and Water Cycle Experiment (GEWEX) Atmospheric Boundary Layer Study (GABLS) test case shown in section 3c.

First, the nonlocal model development of the ACM1, as shown by Pleim and Chang (1992), is described. The model equations are presented here in discrete form on a staggered vertical grid where scalar quantities, such as water vapor, condensed water species, and trace chemical species, as well as horizontal momentum components, are located at the layer centers designated by the subscript i. Vertical fluxes, vertical velocities, and eddy diffusivities are located at the layer interfaces (e.g., $i + ½$). The nonlocal scheme for any scalar C_i (mass mixing ratio) in model layer i is given by

$$\frac{\partial C_i}{\partial t} = \mathrm{Mu}C_1 - \mathrm{Md}_i C_i + \mathrm{Md}_{i+1} C_{i+1} \frac{\Delta z_{i+1}}{\Delta z_i}, \quad (3)$$

which is identical to Eq. (3) in Pleim and Chang (1992), except that here the vertical dimension is expressed as height above ground (z) rather than σ. Here, Mu is the upward convective mixing rate, Md_i is the downward mixing rate from layer i to layer $i - 1$, C_1 is the mixing ratio in layer 1 (the lowest model layer), and Δz_i is the thickness of layer i. The downward mixing rate Md_i is derived from Mu according to mass conservation as

$$\mathrm{Md}_i = \mathrm{Mu}(h - z_{i-1/2})/\Delta z_i, \quad (4)$$

where h is top of PBL. Thus, the flux of C at any model level interface ($i + ½$) is given by

$$F_{i+1/2} = \mathrm{Mu}(h - z_{i+1/2})C_1 - \mathrm{Md}_{i+1}\Delta z_{i+1} C_{i+1}. \quad (5)$$

Combining Eq. (5) with Eq. (4) gives

$$F_{i+1/2} = \mathrm{Mu}(h - z_{i+1/2})(C_1 - C_i). \quad (6)$$

Thus, for the case where C is replaced with virtual potential temperature θ_v, Mu can be defined in terms of kinematic buoyancy flux at the top of the lowest model layer $B_{1.5}$ as

$$\mathrm{Mu} = B_{1.5}/[(h - z_{1+1/2})(\theta_{v1} - \theta_{v2})]. \quad (7)$$

Assuming that the top of the lowest model layer is sufficiently close to the surface that fluxes are dominated by small-scale turbulent eddies; the buoyancy flux can be defined by eddy diffusion as

$$B_{1.5} = K_h(z_{1+1/2}) \frac{(\theta_{v1} - \theta_{v2})}{\Delta z_{1+1/2}}, \quad (8)$$

where the eddy diffusivity K_h is derived from surface layer theory as in Eq. (12), shown below. Combining Eqs. (7) and (8) yields convective mixing rate as a function of K_h:

$$\mathrm{Mu} = \frac{K_h(z_{1+1/2})}{\Delta z_{1+1/2}(h - z_{1+1/2})}. \quad (9)$$

Note that the virtual potential temperature gradient is conveniently eliminated from the convective mixing rate definition. Furthermore, because the convective mixing rate is directly related to eddy diffusivity it is simple to apportion mixing between local and nonlocal components of a combined scheme.

a. Combined local and nonlocal mixing

Combining Eq. (3), which represents the ACM1 nonlocal scheme, with eddy diffusion gives the ACM2 governing equation in discrete form:

$$\frac{\partial C_i}{\partial t} = \mathrm{M2u}C_1 - \mathrm{M2d}_i C_i + \mathrm{M2d}_{i+1} C_{i+1} \frac{\Delta z_{i+1}}{\Delta z_i} + \frac{1}{\Delta z_i}\left[\frac{K_{i+1/2}(C_{i+1} - C_i)}{\Delta z_{i+1/2}} + \frac{K_{i-1/2}(C_i - C_{i-1})}{\Delta z_{i-1/2}}\right]. \quad (10)$$

Note that Mu and Md have been replaced with M2u and M2d since the total mixing is now split between local and nonlocal components by a weighting factor f_{conv}. Thus,

$$\mathrm{M2u} = \frac{f_{\mathrm{conv}} K_h(z_{1+1/2})}{\Delta z_{1+1/2}(h - z_{1+1/2})} = f_{\mathrm{conv}}\mathrm{Mu} \quad \text{and} \quad (11a)$$

$$K(z) = K_z(z)(1 - f_{\mathrm{conv}}). \quad (11b)$$

Vertical eddy diffusivity K_z is defined by boundary layer scaling similarly to Holtslag and Boville (1993) as

$$K_z(z) = k \frac{u_*}{\phi\left(\frac{z_s}{L}\right)} z(1 - z/h)^2, \quad (12)$$

where k is the von Kármán constant (=0.4), u_* is the friction velocity, and h is the PBL height. For unstable conditions ($z_s/L < 0$), $z_s = \min(z, 0.1h)$, and for stable condition $z_s = z$. The nondimensional profile functions for unstable conditions, according to Dyer (1974), are given by

$$\phi_h = \left(1 - 16\frac{z}{L}\right)^{-1/2} \quad \text{and}$$

$$\phi_m = \left(1 - 16\frac{z}{L}\right)^{-1/4}, \quad (13)$$

where the Monin–Obukov length scale L is

$$L = \frac{T_o u_*^2}{gk\theta_*}, \quad (14)$$

T_o represents the average temperature in the surface layer, and θ_* is the surface temperature scale defined as the surface kinematic heat flux divided by u_*. Note that when ϕ in Eq. (12) is replaced by ϕ_h, then K_z becomes K_h. A schematic of the transport between model layers for the ACM2 model is shown in Fig. 1b.

It is clear that f_{conv} is the key parameter that controls the degree of local versus nonlocal behavior. At either extreme ($f_{\mathrm{conv}} = 1$ or $f_{\mathrm{conv}} = 0$) the scheme reverts to either the ACM1 nonlocal scheme or local eddy diffusion, respectively. For stable or neutral conditions f_{conv} is set to zero for pure eddy diffusion because the nonlocal scheme is only appropriate for convective conditions where the size of buoyant eddies typically exceed the vertical grid spacing. Figure 2 shows vertical profiles of potential temperature for a series of 1D simulations where convective conditions are driven by rapidly increasing surface temperature (6 K h^{-1}). The profiles shown are after 6 h of simulation with fixed values of the partitioning factor (f_{conv}) ranging from 0 to 1. The pure eddy diffusion profile ($f_{\mathrm{conv}} = 0$) shows a downward gradient from the ground up to about 1300 m. The eddy diffusion model also results in the highest PBL height. The ACM1 profile ($f_{\mathrm{conv}} = 1$) has a single superadiabatic layer with a near-neutral profile in the lower PBL gradually becoming more stable with height. The other three profiles are in between where the main effect of the nonlocal component seems to be to increase the stability of the lower 2/3 of the PBL and to lower the PBL height. Whereas, adding the local component to the ACM1 leads to a more realistic gradually decreasing superadiabatic profile in the lowest couple hundred meters.

Because the local component depends on the local potential temperature gradient and the nonlocal component does not, the value of f_{conv} determines the height at which the potential temperature gradient goes to zero. As shown in Fig. 2, the higher the value of f_{conv} the lower the level of zero gradient. Of the various proportions of local and nonlocal components tested, the test where $f_{\mathrm{conv}} = 50\%$ seems to give the most realistic results. Figure 3 shows that the normalized flux and potential temperature profiles with $f_{\mathrm{conv}} = 0.5$ are very similar to the LES profiles for the convective boundary layer shown by Stevens (2000). The zero gradient level is about 40% of the PBL height in the ACM2 simulation as compared with about 46% for the LES results shown by Stevens (2000).

The ACM2 equation [Eq. (10)] is similar to Eq. (1) in that the vertical fluxes are described by a combination of a local gradient-driven component and a nonlocal component. There have been many attempts over the years to provide a theoretical basis for this two-component form of the heat flux equation (e.g., Deardorff 1966, 1972; Holtslag and Moeng 1991). For example, Holtslag and Moeng (1991) showed how Eq. (1) can be derived from the second-order heat flux budget equation, albeit with some simplifying parameterizations. Thus, by following the formulation of models based on Eq. (1), an expression for f_{conv} can be derived from the ratio of the nonlocal flux term to the total flux as

$$f_{\mathrm{conv}} = \frac{K_h \gamma_h}{K_h \gamma_h - K_h \frac{\partial \theta}{\partial z}}, \quad (15)$$

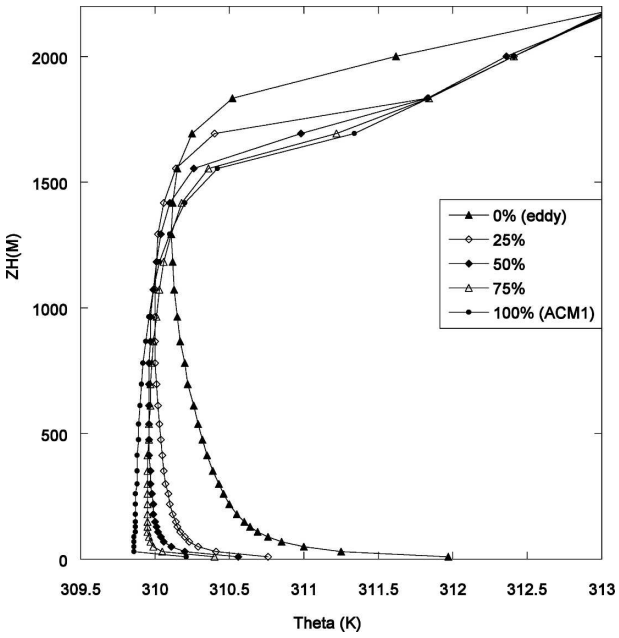

FIG. 2. Potential temperature profiles during convective conditions for various nonlocal fractions of turbulent mixing (f_{conv}).

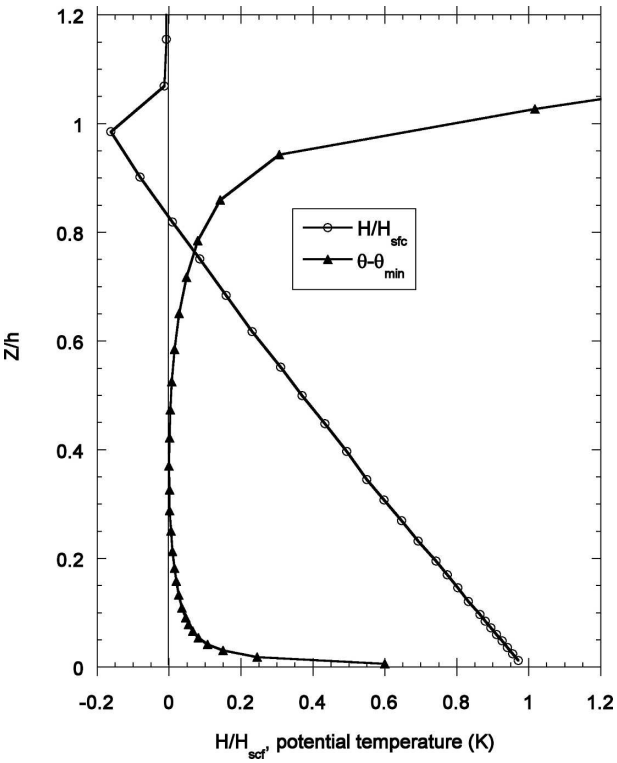

FIG. 3. Normalized sensible heat flux profile and potential temperature profile minus the minimum value using a value of $f_{\text{conv}} = 0.5$.

where γ_h is the gradient adjustment term for the nonlocal transport of sensible heat given by Holtslag and Boville (1993) as

$$\gamma_h = \frac{a w_* (\overline{w'\theta'})_o}{w_m^2 h}, \tag{16}$$

where $w_m = u_*/\phi_m$, w_* is the convective velocity scale, and the constant a is set to 7.2. Substituting Eq. (16) into Eq. (15) and approximating the surface sensible heat flux as

$$(\overline{w'\theta'})_o = -k \frac{u_*}{\phi_h} z_s \frac{\partial \theta}{\partial z}, \tag{17}$$

where $z_s = 0.1h$, gives

$$f_{\text{conv}} = \left(1 + \frac{1}{k0.1a} \frac{u_*}{w_*} \frac{\phi_h}{\phi_m^2}\right)^{-1}. \tag{18}$$

Noting that for the profile functions suggested by Dyer (1974), as shown above in Eq. (13), $\phi_h/\phi_m^2 = 1$, and

$$\frac{u_*}{w_*} = k^{1/3}\left(-\frac{h}{L}\right)^{-1/3};$$

then f_{conv} becomes

$$f_{\text{conv}} = \left[1 + \frac{k^{-2/3}}{0.1a}\left(-\frac{h}{L}\right)^{-1/3}\right]^{-1}. \tag{19}$$

Figure 4 shows how f_{conv}, defined according to Eq. (19), behaves as a function of stability. Using this function for partitioning the local and nonlocal components of the model for all unstable conditions allows for a gradual transition from stable and neutral conditions, where local transport only is used, through increasing instability where the nonlocal component ramps up very quickly but then levels off at around 0.5. This agrees with the test results shown in Figs. 2 and 3 that suggest for strongly convective conditions f_{conv} should have a maximum value of about 0.5.

Because the f_{conv} is derived from the model described by Holtslag and Boville (1993, hereinafter HB93), which is an example of a model represented by Eq. (1), the eddy diffusivity used in ACM2, defined by the combination of Eqs. (11b), (12), and (18), is identical to the eddy diffusivity for heat in the HB93 model when the nonlocal term is included in the definition of the Prandtl number (see HB93, their appendix A). Thus, the eddy diffusion terms are the same while the countergradient term in Eq. (1) ($K_z\gamma$) is replaced by the transilient terms that involve the nonlocal mass exchange rates (M2u and M2d). The advantage of the ACM2 approach is that the nonlocal mass exchange is

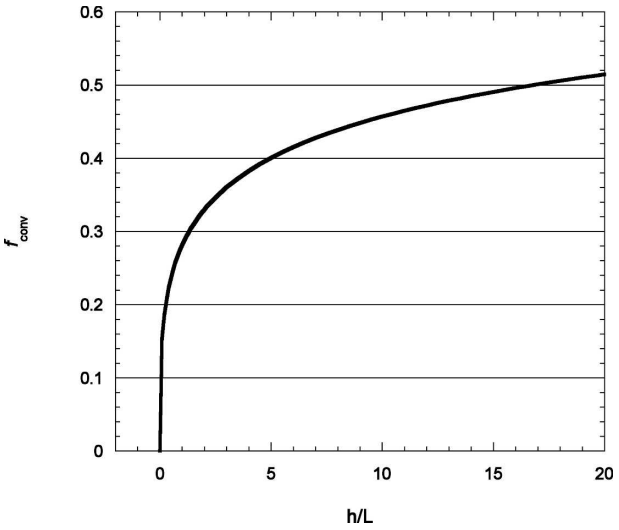

FIG. 4. Nonlocal fraction of turbulent mixing (f_{conv}) as a function of stability.

a physical representation of upward transport by detraining convective plumes that applies to any quantity, whereas the models represented by Eq. (1) adjust the local potential temperature gradient to account for the effects of large-scale convection driven by the surface heat flux. While such models work well for heat where surface heat flux is both the source of the transported quantity and the driver of the convective turbulence, for other transported quantities the surface heat flux in Eq. (16) is replaced by the surface flux of the transported quantity. Thus, nonlocal effects are proportional to the surface flux, which may be driven by mechanisms completely unrelated to convective turbulence (e.g., chemical emissions from mobile or area sources). Furthermore, for quantities that have no upward surface fluxes (e.g., ozone) these models revert to eddy diffusion only, but with an eddy diffusivity (assumed to be the same as for heat) diminished by the nonlocal term in the Prandtl number equation.

b. Diagnostic scheme for determination of PBL height

Many models (e.g., Troen and Mahrt 1986; Holtslag and Boville 1993) diagnose the PBL height h by incremental calculation of the bulk Richardson number Ri_b from the surface up to a height at which $\text{Ri}_b > \text{Ri}_{\text{crit}}$. An advantage of this method is that it can be used for all stability conditions, with the idea that the PBL should be defined as a bulk layer where turbulence predominates. For unstable conditions, however, the PBL should be considered as composed of a free convective layer whose top is the level of neutral buoyancy with respect to a rising thermal of surface layer air, and as an entrainment zone that is statically stable but turbulent because of penetrating thermals and wind shear. Thus, the bulk Richardson number method should be applied over the entrainment layer only. In this way, h is diagnosed as the height above the level of neutral buoyancy where Ri_b computed for the entrainment layer exceeds the critical value. The advantage of this technique is that the wind shear in the entrainment zone is considered explicitly rather than the wind speed at height h. Also, the height above ground is not a relevant parameter in this method, whereas the thickness of the stable entrainment layer is.

For stable conditions the method for diagnosis of PBL height h is the same as for the previous models:

$$h = \text{Ri}_{\text{crit}} \frac{\overline{\theta_v} U(h)^2}{g[\theta_v(h) - \theta_v(z_1)]}, \tag{20}$$

where θ_v is the virtual potential temperature, z_1 is the height of the lowest model level, and $\overline{\theta_v}$ is the average virtual potential temperature between the layer 1 and h. For unstable conditions, first the top of the convectively unstable layer (z_{mix}) is found as the height at which $\theta_v(z_{\text{mix}}) = \theta_s$ [where

$$\theta_s = \theta_v(z_1) + b \frac{(\overline{w'\theta_v'})_o}{w_m}$$

and $b = 8.5$, as suggested by Holtslag et al. (1990)]. The bulk Richardson number is then defined for the entrainment layer above z_{mix} such that

$$\text{Ri}_b = \frac{g[\theta(h) - \theta_s](h - z_{\text{mix}})}{\overline{\theta_v}[U(h) - U(z_{\text{mix}})]^2}. \tag{21}$$

The top of the PBL is diagnosed as the height h where Ri_b, computed according to Eq. (21), is equal to Ri_{crit}. Note that for some of the LES testing described in the next section this modified method for diagnosis of PBL height gave significantly better results, but in MM5 applications the difference was very small.

3. Testing and evaluation

A good PBL model for use in mesoscale meteorological and air-quality modeling should be able to accurately simulate the morning growth, maximum height, and evening collapse of the PBL while predicting realistic profiles of temperature, humidity, winds, and other scalar quantities. In a full 3D meteorological model, simulations are affected by many components of the model dynamics and physics, such as radiation, cloud cover, land surface modeling, and large-scale subsidence, thus confounding evaluation of the PBL scheme. Therefore, testing of a PBL scheme should start with controlled offline experiments where initial

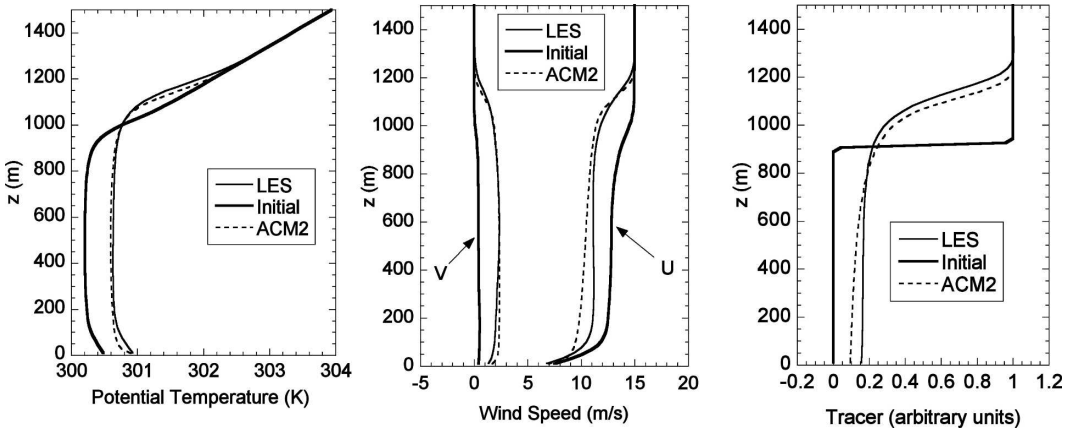

FIG. 5. (left) Potential temperature, (middle) wind speed, and (right) tracer profiles by LES and the ACM2 for experiment 05WC.

conditions and surface and dynamic forcings are specified. LESs provide good benchmarks for this type of testing as shown in the next section, but LESs generally represent quasi-steady conditions and, therefore, do not test the diurnal evolution of PBL simulations. The next step in testing is 1D simulations over multiple days and comparisons with field measurements, as shown below in section 3c. Evaluation of the ACM2 in a mesoscale meteorological model will follow in Part II of this paper and evaluation of the ACM2 in an air-quality model will follow in a subsequent publication.

a. LES testing

A common approach for testing PBL models is by comparison with LESs (e.g., Hourdin et al. 2002; Noh et al. 2003). While LESs are high-resolution time-dependent model simulations, quasi-steady PBL profiles can be obtained by horizontally averaging across the whole computational grid, using periodic boundary conditions, and averaging in time over many large-eddy turnover time periods ($\tau = z_i/w_*$). Ayotte et al. (1996) ran a series of LES experiments that were used for comparison with 16 different 1D PBL schemes. The experiments represented cloud-free PBLs driven by shear and buoyancy. Various stability and wind shear conditions were generated using constant prescribed forcing by surface heat flux and geostrophic wind profiles. After a period of $\sim 5\tau$ to spin up turbulent dynamics, passive tracers were added to the simulations and the LES were run for another $\sim 10\tau$, wherein the last 6τ were averaged to produce the final profiles. The PBL schemes were initialized from the LES profiles after the 5τ spinup, run for $\sim 10\tau$, and averaged over the final 6τ for comparison with LES final profiles. See Ayotte et al. (1996) for a detailed description of the LES model and the simulation experiments.

Three of the 10 cases were chosen to test the ACM2—one had a weak capping inversion and a low value of surface sensible heat flux ($Q_* = 0.05$ K m s^{-1}), designated as 05WC, and two had strong capping inversions with low ($Q_* = 0.05$ K m s^{-1}) and high ($Q_* = 0.24$ K m s^{-1}) values of surface sensible heat flux, labeled 05SC and 24SC, respectively. All three cases had a roughness length of 0.16 m, with $U_g = 15.0$ m s^{-1} and $V_g = 0.0$ at all levels, and were dry (thus, $\theta = \theta_v$). The vertical grid used for the ACM2 simulation is identical to the LES vertical grid.

Figure 5 shows potential temperature, u and v wind components, and tracer profiles for the 05WC experiment. The initial profiles were produced after a 3936-s spinup period ($\sim 5\tau$) and used to initialize the ACM2 simulation. The ACM2 and LES results were compared for an averaging period between 3800 and 9120 s after the initial state. Note that this was the most difficult of the three experiments to replicate because of the weak surface forcing and the weak capping inversion. However, the ACM2 results compare very closely to the LES results. The slight deviation from the final LES potential temperature profile is a small cool bias in the mixed layer and slightly less penetration into the capping inversion. The v-wind-component profiles show very close agreement, while for the u-wind-component profiles the ACM2 results show a bit more gradient in the middle portion of the PBL. The scalar results also show a tendency to underpredict the upward extent of the mixing and the degree of mixing in the lower portion of the PBL. Note that these results could be made to compare more exactly by adjustment of the f_{conv} parameter and the minimum K_z (now set to 0.1 m^2 s^{-1}), but such "tuning" may degrade results of the other experiments.

Figure 6 shows the results of the 05SC experiment

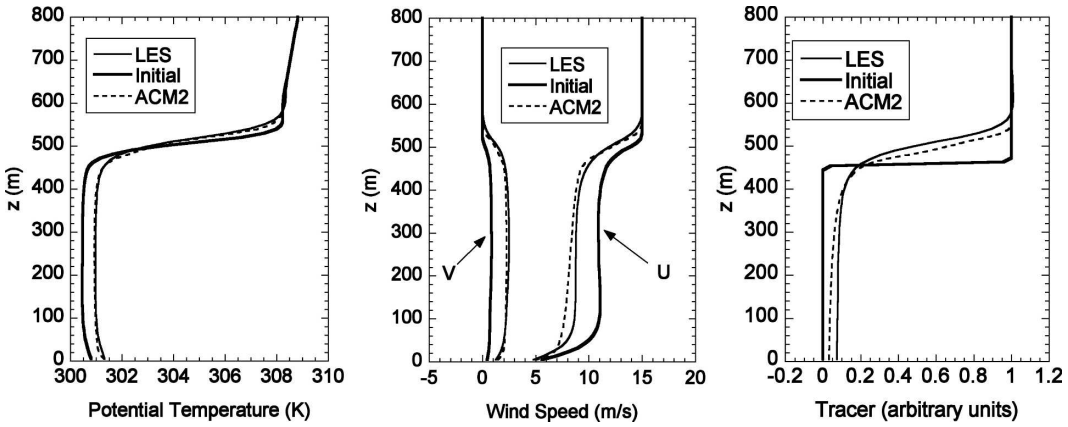

FIG. 6. Same as Fig. 5, but for experiment 05SC.

that differ from those of 05WC, primarily in the strength of the capping inversion. The combination of weak surface forcing and a strong constraint on the extent of mixing makes for smaller differences between the ACM2 and LES results. The potential temperature and v-component wind profiles compare almost exactly, while the u-component and scalar profiles again show that the ACM2 profiles have slightly greater gradients in the middle levels of the PBL than the LES results.

The third experiment, 24SC, has a similar strong capping inversion as experiment 05SC but with much greater surface heat flux ($Q_* = 0.24$ K m s^{-1}). The results of this experiment (Fig. 7) also show that the ACM2 compares very closely to the LES. The θ and v profiles again show better agreement than the u and tracer profiles. The same tendency toward slightly more gradient in the lower PBL is evident for u and the tracer. The LES results show a curious bulge in the θ and tracer profiles just above the top of the PBL. It is clear that this feature cannot be reproduced by a mass-conservative mixing scheme such as the ACM2.

Figure 8 shows vertical profiles of sensible heat flux from both the LES and the ACM2 simulations for experiment 24SC. Three profiles are shown for the ACM2 simulations: local and nonlocal components and the total. Vertical fluxes of any quantity C can be computed in the ACM2 scheme as

$$F_c = M(h - z_{i+1/2})(C_1 - C_i) + K_i\left(\frac{C_{i+1} - C_i}{\Delta z_{i+1/2}}\right), \quad (22)$$

where the first term on the right-hand side represents the nonlocal component and the second term is the local component. According to the results shown in Fig. 8, most of the upward heat flux in the lower and middle parts of the PBL is carried by the nonlocal component. The local component turns negative (downward) about half way up and is responsible for most of the negative fluxes in the entrainment zone. Thus, the magnitude of the entrainment flux, which in this case is underestimated, is largely dependent on the magnitude of the eddy diffusivity near the top of the PBL. Testing showed that entrainment fluxes, and thus PBL growth into the capping inversion, are very sensitive to the

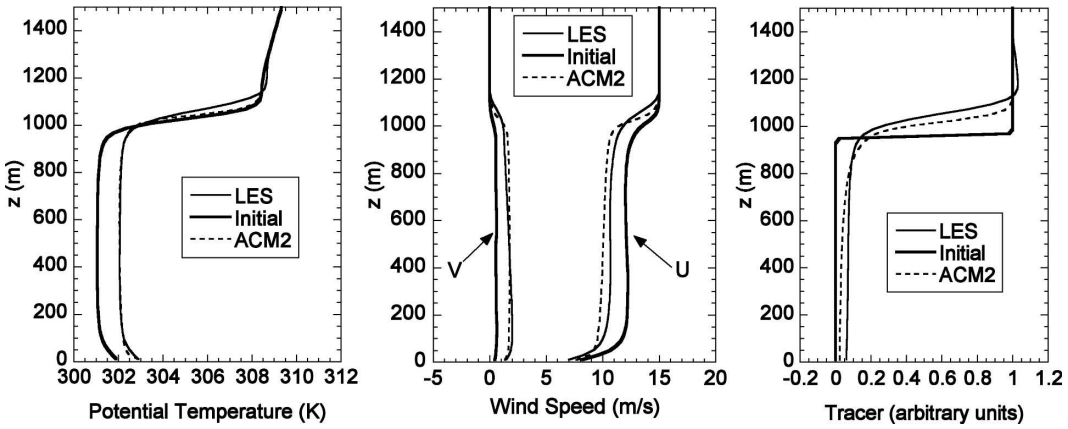

FIG. 7. Same as Fig. 5, but for experiment 24SC.

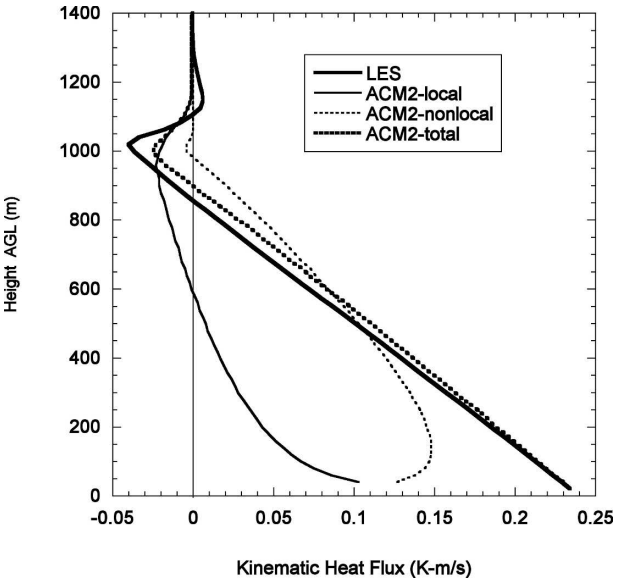

FIG. 8. Profiles of sensible heat flux. Local, nonlocal, and total sensible heat flux are compared with LES sensible heat flux.

minimum value specified for K_z. It was also found that using the maximum of the PBL scaling form for K_z [Eq. (12)] and a local formulation that accounts for vertical wind shear was an important improvement for getting good agreement at the top of the PBL. The formulation for the local scaling version of eddy diffusivity is shown in Part II.

b. Comparisons with other PBL models

To get a better understanding of the ACM2's capabilities, it is useful to compare with other PBL models. These LES experiments provide an excellent controlled laboratory for such comparisons. The 05WC case is selected for comparisons between the ACM2, the ACM1, and the HB93 model. This set of models was chosen because they are closely related and therefore easily comparable. The ACM2 has the same nonlocal component as the ACM1 (although diminished by f_{conv}), while the HB93 model has the same eddy diffusion component as the ACM2, but with a different form of nonlocal parameterization. It is interesting to see what advantage the addition of the eddy diffusion component affords over the purely nonlocal ACM1 scheme. Also, the comparison with HB93 shows the relative validity of the ACM1 approach to nonlocal effects versus the gradient adjustment approach for heat, momentum, and two types of tracers. Note that all three schemes are run using identical modeling infrastructure, including surface layer parameterizations and PBL height calculations, in order to directly compare transport algorithms. Therefore, because the eddy diffusion plus the countergradient term model is not run exactly as described by HB93, it is referred to eddy plus nonlocal (EDDYNL) rather than HB93 to make clear that the results shown are not exactly what the HB93 model would produce.

Figure 9 shows the potential temperature, the u and v wind components, the same tracer shown in Figs. 5–7 that is designated C, and an additional tracer that has a nonzero surface boundary condition, designated B. The initial profiles have been omitted from each plot, and the scale on the potential temperature plot (Fig. 9a) has been expanded. Note that the EDDYNL model includes a nonlocal term for potential temperature and the B tracer only. The nonlocal term for potential temperature is given by Eq. (16) and for the B tracer when the surface heat flux is replace by the B flux resulting from the surface boundary condition ($B_{\text{surf}} = 15$ arbitrary units).

While all three models compare reasonably well to the LES results for potential temperature, the ACM2 results are closest to the LES profile both at the surface and near the top of the neutral layer. The EDDYNL model profile has a similar shape but is a bit warm at the surface, cool at the top of the neutral layer, and a little low for PBL height. Note that if the PBL height is computed as described by HB93, the resulting profile shows a much higher PBL that is even higher than the LES result (not shown). The ACM1 shows a small cool bias at the surface and warm bias with more stable gradient near the top of the neutral layer. Comparison between ACM2 and ACM1 shows the importance of the eddy diffusion component for realistic gradients in the surface layer.

The wind profiles (Fig. 9b) show more distinct difference among the models, especially for the u component. The ACM2 u component profile has a shape most closely resembling the LES results, even though it has more gradient in the middle portion of the PBL. While the ACM1 u profile is the most nearly constant with height through most of the mixed layer, like the LES, it has a considerable low bias throughout most of the PBL. The EDDYNL shows the most diffusive u profile and further evidence of an underpredicted PBL height. Note that Noh et al. (2003) have implemented a nonlocal term for momentum in a similar model that shows improved u profile results for similar LES experiments that are much like the ACM2 results shown here. These results suggest that both local and nonlocal components are important for momentum transport because the shape and magnitude of the ACM2 profile is closer to the LES profile than either the ACM1, which has no local component, or EDDYNL, which has no nonlocal component. However, even the ACM2 profile shows considerable discrepancy from the LES result, suggesting that intermediate scales of turbulent eddies that are

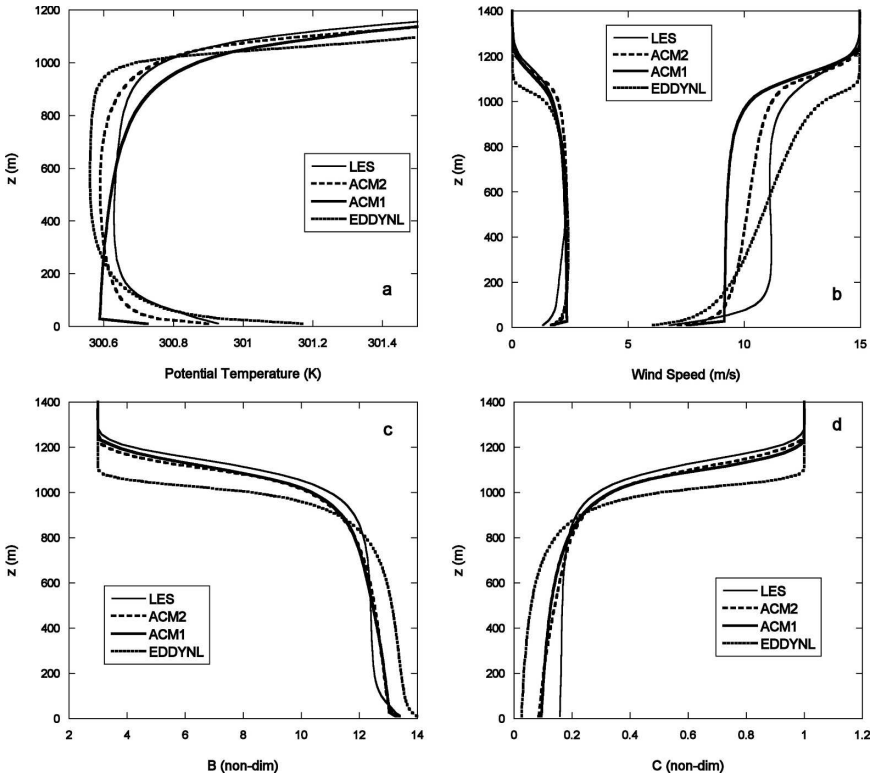

FIG. 9. Comparison of ACM2, ACM1, and EDDYNL (Holtslag and Boville 1993) with the 05WC LES experiment for (a) potential temperature, (b) wind components, (c) *B* tracer, and (d) *C* tracer.

neglected in this scheme may be important for momentum transport in the mid-PBL layers.

The *C* tracer results (Fig. 9c) show almost identical profiles for ACM1 and ACM2, but with a bit more gradient than the LES profile and lower values near the surface. The EDDYNL profile shows even lesser values in the lower layers because of the lower PBL height that results in less entrainment of the higher *C* values aloft. The *B* tracer profiles, shown in Fig. 9d, also show close similarity between ACM1 and ACM2, but with a more continuous curve in the lowest layers for ACM2. The near-surface overprediction by the EDDYNL model is again attributable to the underprediction of PBL height. As with the *C* tracer profiles, all three models produce *B* tracer profiles with more gradient in the mid-PBL layers than the LES. This may again reflect the inability of these simple models to include the full range of eddy scales between the subgrid scales that drives the eddy diffusion term and the PBL scale of the nonlocal components.

c. GABLS experiment

The second intercomparison project from the GABLS is based on 3 days from the Cooperative Atmosphere–Surface Exchange Study 1999 (CASES-99) experiment and aims to study the representation of the diurnal cycle over land in both 1D column models and LESs. Simple initial conditions and forcing in the form of surface temperature, geostrophic wind velocity, and large-scale subsidence were provided. The ACM2 was one of 23 1D models that simulated the experiment. The experiment setup and preliminary results of the model intercomparison and evaluation through comparison with observations can be found online (http://www.misu.su.se/~gunilla/gabls/). The results shown here are limited to comparison of the ACM2 simulations with CASES-99 measurements.

Figure 10 shows the 2-m air temperature simulated by the ACM2 along with measurements at 1.5 m on the main tower and 2 m from six surrounding towers. The model results follow the measurements very closely with the exception of the lowest temperatures on the second night (hours 46–52). Daytime peak temperatures are especially well simulated. The 10-m wind speed simulated by the ACM2, however, departs significantly from the observations, especially during the daytime (Fig. 11). There is good agreement during the early morning hours (24–32) with an abrupt jump

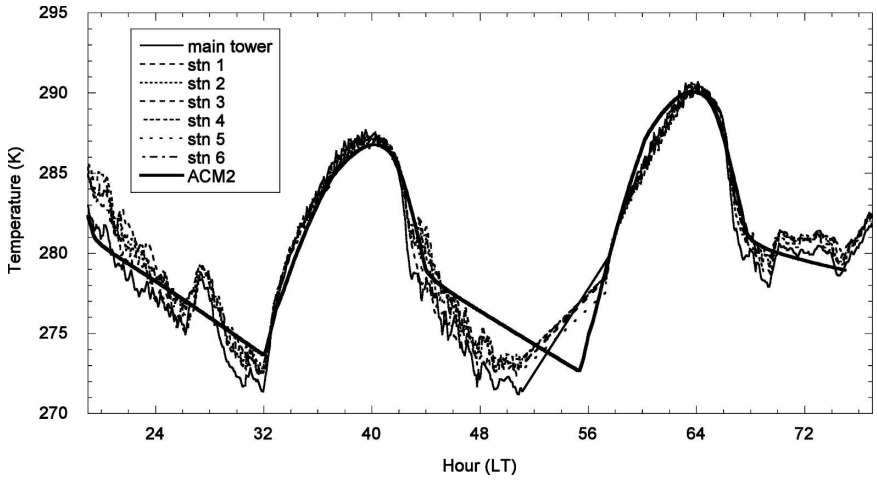

FIG. 10. The 2-m temperature for the GABLS experiment simulated by the ACM2 in comparison with measurements at seven towers from the CASES-99 experiment.

around 0900 LT. The observations show higher wind speeds during the day that are fairly constant (4–6 m s^{-1}), while the ACM2 has a morning dip and afternoon peak. According to the preliminary analysis of the GABLS model intercomparison presented by Svensson and Holtslag (2006) the ACM2 produced the highest peak afternoon wind speed of all of the models tested. Clearly, winds are very difficult to model with a 1D simulation using a very simple setup and constant geostrophic forcing. However, one of the things to look for in the MM5 simulations, discussed in Part II, will be evidence of afternoon overpredictions in wind speed.

The surface sensible heat flux simulated by the ACM2 is compared with eddy covariance measurements at 1.5 m on the main tower and shown in Fig. 12. Except for some morning underprediction, the modeled heat fluxes compare very well to the measurements. Figures 13 and 14 show potential temperature and wind speed from a radiosonde launched at 1900 UTC 23 October 1999 (hour 38) from Leon, Kansas, (about 5 km northwest of the main tower) in comparison with the ACM2 simulations. These soundings show that the ACM2 has produced a very accurate afternoon PBL height. The lower part of the potential temperature profile, however, seems to show some discrepancy in the gradient near the surface. To examine this further, Fig. 15 shows temperature measurements at six heights on the 55-m main tower and demonstrates that

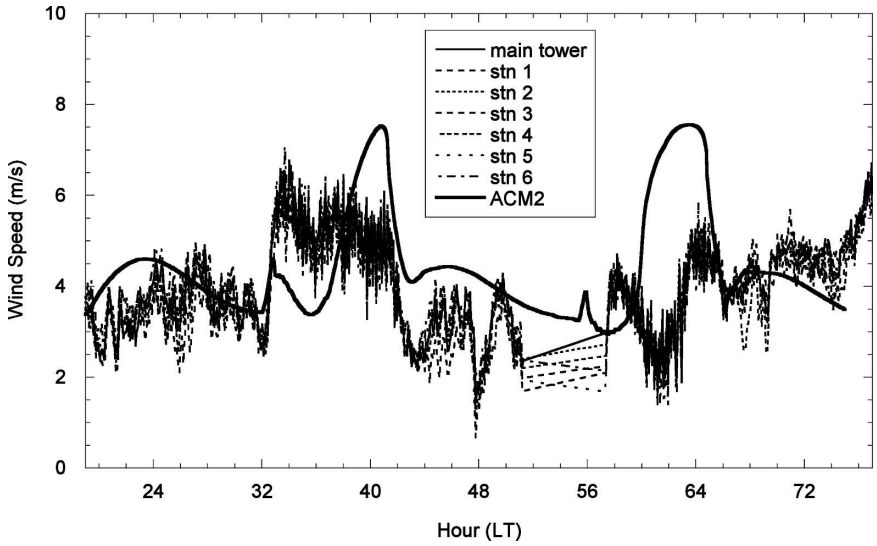

FIG. 11. Same as Fig. 10, but for 10-m wind speed.

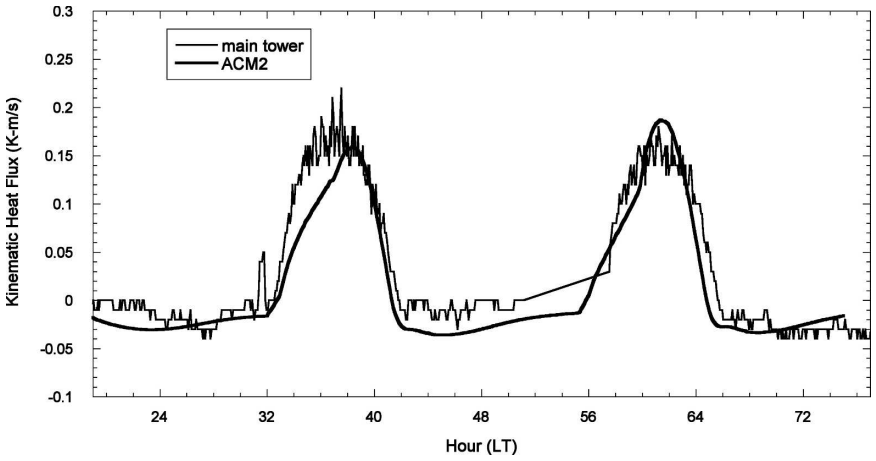

FIG. 12. Surface sensible heat flux from the ACM2 simulation and measured at 1.5-m height on the main tower of the CASES-99 experiment (23–24 Oct 1999).

the near-surface profile produced by the ACM2 is fairly accurate. Note that the ability to produce such curving gradients near the surface is one of the key improvements over the original ACM1.

4. Summary

Both the LES and GABLS experiments demonstrate that the ACM2 is able to simulate realistic PBL heights, temperature profiles, and surface heat fluxes. The ACM2 provides a simple solution to the problem of modeling both the small- (subgrid) and large-scale turbulent transport within convective boundary layers. As a consequence, the profiles of both heat flux and potential temperature can be realistically simulated. For the turbulent transport of heat in the convective boundary layer the ACM2 has similar capabilities to the modified eddy diffusion scheme with the gradient adjustment term. In fact, the same formulation for the gradient adjustment term is used for deriving the partitioning of the local and nonlocal mixing components in the ACM2. The advantage of the ACM2 is that the local and nonlocal mixing rates are defined in terms of the bulk physical characteristics of the PBL and are equally applicable to any transported quantity.

The LES experiments show that the importance of adding the eddy diffusion component to the original ACM1 is most evident for quantities that have large

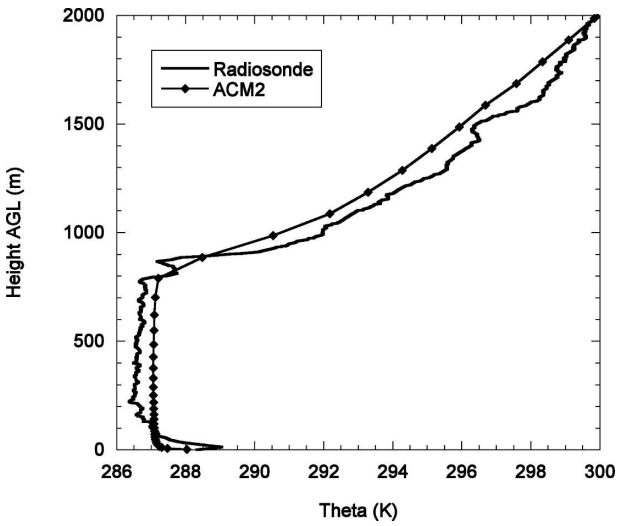

FIG. 13. Potential temperature profiles from the ACM2 simulation and a rawinsonde launched from Leon at 1900 UTC (1400 LT) 23 Oct 1999.

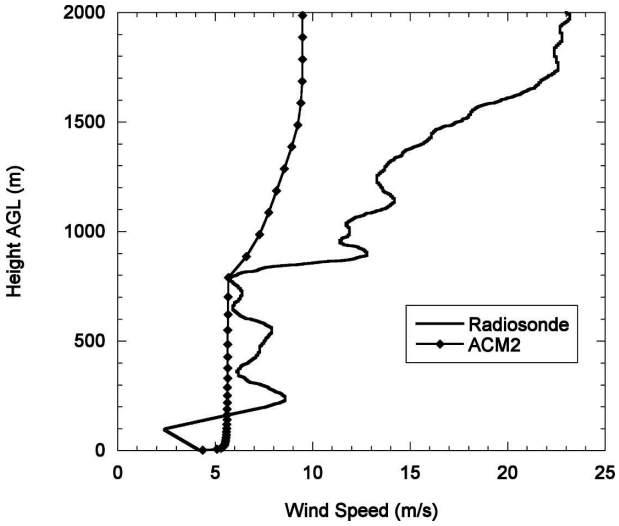

FIG. 14. Wind speed profiles from the ACM2 simulation and a rawinsonde launched from Leon at 1900 UTC (1400 LT) 23 Oct 1999.

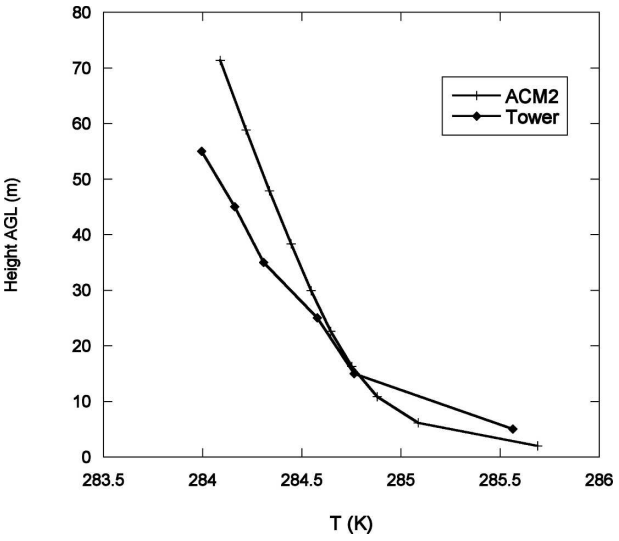

FIG. 15. Temperature profiles from the ACM2 simulation and the 55-m main CASES-99 tower at 1900 UTC (1400 LT) 23 Oct 1999.

surface fluxes (either positive or negative), such as heat and momentum. Simulation of realistic profiles of such quantities in the surface layer clearly requires a downgradient flux component. The profiles of the *B* and *C* tracers, on the other hand, showed very little difference between ACM2 and ACM1.

The ACM2 has been incorporated into the MM5 and coupled to the Pleim–Xiu land surface model. The ACM2 is also being added as a PBL model option to the WRF model. The capabilities of the ACM2 for use in mesoscale meteorological modeling are demonstrated in Part II, and the capabilities of the ACM2 for use in air-quality modeling will be demonstrated in a future paper.

Acknowledgments. The author thanks Keith Ayotte for providing the results of his large-eddy simulations. The author also acknowledges the chair of GABLS Prof. Bert Holtslag and the coordinator of the second intercomparison experiment Dr. Gunilla Svensson for organizing the GABLS experiment and providing the setup and description of the modeling study. The research presented here was performed under the Memorandum of Understanding between the U.S. Environmental Protection Agency (EPA) and the U.S. Department of Commerce's National Oceanic and Atmospheric Administration (NOAA) and under Agreement DW13921548. This work constitutes a contribution to the NOAA Air Quality Program. Although it has been reviewed by EPA and NOAA and approved for publication, it does not necessarily reflect their policies or views.

REFERENCES

Ayotte, K. W., and Coauthors, 1996: An evaluation of neutral and convective planetary boundary-layer parameterizations relative to large eddy simulations. *Bound.-Layer Meteor.,* **79,** 131–175.

Blackadar, A. K., 1978: Modeling pollutant transfer during daytime convection. Preprints, *Fourth Symp. on Atmospheric Turbulence, Diffusion, and Air Quality,* Reno, NV, Amer. Meteor. Soc., 443–447.

Byun, D., and K. L. Schere, 2006: Review of the governing equations, computational algorithms, and other components of the models-3 Community Multiscale Air Quality (CMAQ) modeling system. *Appl. Mech. Rev.,* **59,** 51–77.

Deardorff, J. W., 1966: The counter-gradient heat flux in the lower atmosphere and in the laboratory. *J. Atmos. Sci.,* **23,** 503–506.

——, 1972: Theoretical expression for the counter-gradient vertical heat flux. *J. Geophys. Res.,* **77,** 5900–5904.

Dyer, A. J., 1974: A review of flux-profile relationships. *Bound.-Layer Meteor.,* **7,** 363–372.

Grell, G. A., J. Dudhia, and D. Stauffer, 1994: A description of the fifth-generation Penn State/NCAR Mesoscale Model (MM5). NCAR Tech. Note TN-398+STR, 138 pp.

Holtslag, A. A. M., and C.-H. Moeng, 1991: Eddy diffusivity and countergradient transport in the convective atmospheric boundary layer. *J. Atmos. Sci.,* **48,** 1690–1698.

——, and B. A. Boville, 1993: Local versus nonlocal boundary-layer diffusion in a global climate model. *J. Climate,* **6,** 1825–1842.

——, E. I. F. De Bruijn, and H.-L. Pan, 1990: A high resolution air mass transformation model for short-range weather forecasting. *Mon. Wea. Rev.,* **118,** 1561–1575.

Hourdin, F., F. Couvreux, and L. Menut, 2002: Parameterization of the dry convective boundary layer based on a mass flux representation of thermals. *J. Atmos. Sci.,* **59,** 1105–1123.

Noh, Y., W. G. Cheon, S. Y. Hong, and S. Raasch, 2003: Improvement of the K-profile model for the planetary boundary layer based on large eddy simulation data. *Bound.-Layer Meteor.,* **107,** 401–427.

Pleim, J. E., 2007: A combined local and nonlocal closure model for the atmospheric boundary layer. Part II: Application and evaluation in a mesoscale meteorological model. *J. Appl. Meteor. Climatol.,* **46,** 1396–1409.

——, and J. S. Chang, 1992: A non-local closure model for vertical mixing in the convective boundary layer. *Atmos. Environ.,* **26A,** 965–981.

Stevens, B., 2000: Quasi-steady analysis of a PBL model with an eddy-diffusivity profile and nonlocal fluxes. *Mon. Wea. Rev.,* **128,** 824–836.

Stull, R. B., 1984: Transilient turbulence theory. Part I: The concept of eddy-mixing across finite distances. *J. Atmos. Sci.,* **41,** 3351–3367.

Svensson, G., and A. A. M. Holtslag, 2006: Single column modeling of the diurnal cycle based on CASES99 data—GABLS second intercomparison project. Preprints, *17th Symp. on Boundary Layers and Turbulence,* San Diego, CA, Amer. Meteor. Soc., CD-ROM, 8.1.

Troen, I., and L. Mahrt, 1986: A simple model of the atmospheric boundary layer: Sensitivity to surface evaporation. *Bound.-Layer Meteor.,* **37,** 129–148.